Visualization and Quantification of Rotor Tip Vortices in Helicopter Flows

David L. Kao[1], Jasim U. Ahmad[2], Terry L. Holst[3]
NASA Ames Research Center, Moffett Field, CA

This paper presents an automated approach for extraction, visualization, and quantification of vortex core radii from the Navier-Stokes simulations of a UH-60A rotor in forward flight. We adopt a scaled Q criterion to determine vortex regions and then perform vortex core profiling in these regions to calculate vortex core radii. In particular, the vortex core radii are displayed graphically in a plane using a new color map scheme. This method represents an efficient way of visualizing and quantifying rotorcraft vortical flow fields.

I. Introduction

Helicopter aeromechanics encompasses a highly vortical flow field. The vortices generated at each blade tip contain unsteady, complex, three-dimensional structures, which interact with each other, other blades, the fuselage and various components of the helicopter. It is crucial to understand vortex kinematics and their subsequent dynamic evolution. Much research has been devoted to the understanding of helicopter vortex dynamics, including a number of experimental studies.[1-6]

In May 2010 Particle Image Velocimetry (PIV) measurements of a full-scale UH-60A rotor were acquired in the National Full-Scale Aerodynamics Complex (NFAC) 40- by 80-Foot Wind Tunnel.[1] These measurements were taken at a plane just downstream of the advancing blade in the vicinity of the blade tip—the so-called PIV plane. The resulting PIV data were then processed using an ensemble-average approach to create graphical representations of the vortical wake velocity and vorticity fields, which, in turn, have enhanced the understanding of rotorcraft vortical wake flow field physics and have provided a more detailed validation of vortical wake computer simulations.[7]

A common approach used to analyze flow field features is to compute and plot color contour maps of various scalar quantities such as pressure, velocity magnitude and vorticity magnitude. For example, the color map of the vorticity magnitude is typically used to determine vortical flow structure. With this approach the vortex core may appear larger or smaller, depending on the contour levels that are selected. Thus, the resulting visualization is sensitive to user-specified contour levels. For vortex core radius measurements, it is more accurate to calculate the vortex core radius using the cross-flow velocity profile across the vortex core. The task of extracting the cross-flow velocity profile can be time consuming with existing tools since the user needs to manually select the core center then specify sampling points along the profile axis. The task becomes even more challenging when the associated grid system uses AMR (Adaptive Mesh Refinement) where the profile axis could span multiple grid blocks. There are a number of existing techniques for profiling of vortex core attributes;[8-9] however, these techniques are not fully automatic in that the user still needs to select the vortex core center to compute the cross-flow velocity profile.

The present study introduces a new color map scheme that is based on the vortex core radius, which is fully automatic and does not require user intervention. Analysis and visualization of blade tip vortices on the PIV plane using the proposed new color map scheme are described in Section II. The new approach is evaluated using two case studies, which are described in Section III. The paper ends with a summary in Section IV.

II. Approach

A. Computational PIV Plane

For analyzing computational results using experimental PIV data, it is convenient to represent the experimental PIV plane using a Cartesian grid. This Cartesian plane is hereafter referred to as the *view plane*. In the experimental

[1] Researcher, NASA Advanced Supercomputing Division, M/S N258-5, Member AIAA.
[2] Aerospace Engineer, NASA Advanced Supercomputing Division, M/S N258-2, Member AIAA.
[3] Branch Chief, Fundamental Modeling and Simulation Branch, NASA Advanced Supercomputing Division, M/S N258-2, AIAA Fellow.

setup of Ref. 1, the PIV plane, 3.5 ft. high by 14 ft. wide, is parallel to the model YZ plane and is 21.5 inches downstream of the advancing-blade trailing edge when the advancing blade is at an azimuth of 90° (when the blade is along the positive Y-direction). In this context the X-coordinate is positive downstream, the Y-coordinate is positive to the pilot's right, and the Z-coordinate is positive up.

The simulation to be analyzed utilizes a multi-zone structured overset grid system,[10] which is comprised of a set of curvilinear grids, called near-body (NB) grids, that are generated next to each aerodynamic surface, and a set of Cartesian grids, called off-body (OB) grids, that are generated in the flow domain for all regions away from the aerodynamic surfaces. The OB grids are automatically generated within the OVERFLOW flow solver according to user specified input parameters.[11] Moreover, the OB grids are generated at various levels of resolution starting from "Level 1" (the L1 grid) in the rotor wake region, to successively coarser grid levels (L2, L3, L4, … etc.) that rapidly and efficiently extend the grid system to the far field. The view plane is constructed from the L1 grid using a simple extraction/interpolation algorithm. Figures 1 and 2 illustrate the position of the view plane relative to the L1 grid system for two datasets. In Fig. 1, the view plane spans across two L1 computational grid zones. Note that the advancing rotor blade has advanced by 5° beyond the X=0 plane, that is, the advancing blade is at an azimuth of 95°. In Fig. 2, the view plane spans across many zones for a simulation in which AMR was used.

To determine the vortex core radius at a point near a vortex center, it is necessary to obtain the cross-flow velocity along a line that crosses the vortex core center.[8-9] To facilitate this process, especially for cases in which multiple L1 grid zones are involved, a "finest-grid" view plane is constructed with a grid spacing equal to that of the finest L1 grid. The velocity components at the resulting view plane grid points are then determined using tri-linear interpolation. This ensures that flow field detail from the finest grid will not be missed.

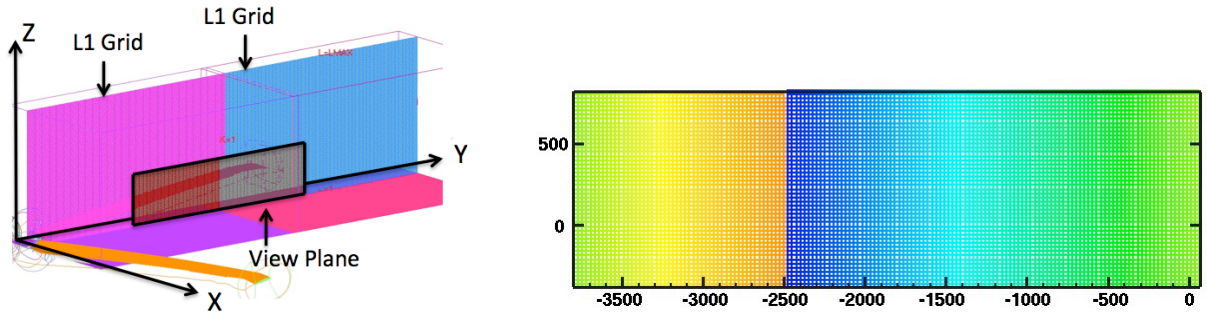

Figure 1. (a) The view plane spans across just two L1 off-body grids and coincides with the *x=c* plane, where *c=21.5* inches. (b) The view plane from (a) is represented by interpolated grid points from the two L1 grids and is color-mapped by the grid point index number.

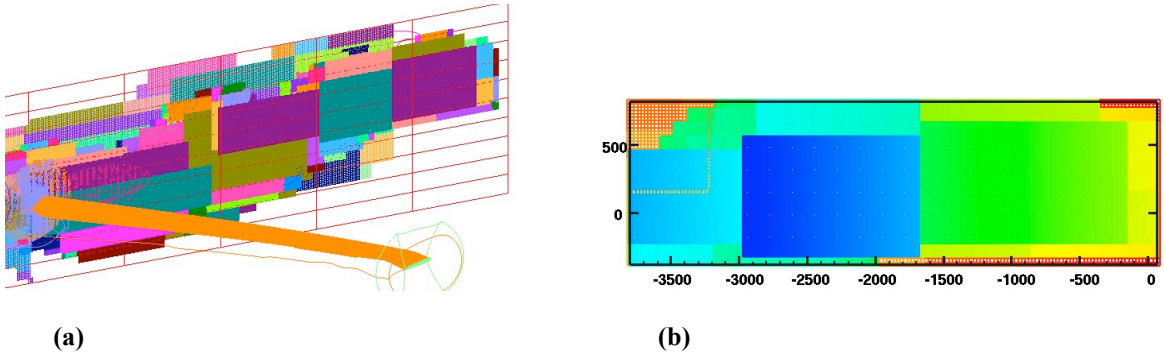

Figure 2. (a) The view plane spans across many L1 off-body grids in an AMR grid case. (b) The view plane is represented by interpolated grid points from many L1 grids and is color-mapped by the grid point index number.

B. Cross-flow Velocity Profiling

The next step is to calculate the vortex core radius from the cross-flow velocity components. A typical approach is to plot a cross-flow velocity profile across a vortex core. Then, the core diameter can be obtained by calculating the distance between the cross-flow velocity component minimum and maximum values. One challenge with this approach is that the user needs to manually select a vortex core center. This task can be time consuming and inaccurate. A second challenge with this approach is that the vortex filament may not be perpendicular to the PIV plane. Thus, a more accurate approach is to plot the cross-flow velocity component along a direction that is orthogonal to the vortex filament. Finding this direction can be difficult and is also prone to error. A third difficulty with this approach occurs when the vortex core is not circular in shape. The use of multiple cross-flow velocity component profiles, each of which is orthogonal to the vortex core, will solve this problem. For example, one could use a plot of the z-component of velocity along the y-direction and a plot of the y-component of velocity along the z-direction. The final vortex core radius is then obtained by averaging the core radii calculated from the two cross-flow velocity profiles.

A main contribution of the present work is to develop a way for selecting a minimal set of grid points to perform the cross-flow velocity component profiling. This methodology is developed using a baseline simulation involving the UH-60A rotor system with the fuselage, wind tunnel walls and model supports all modeled. The flow conditions include an advance ratio of 0.15 and a tip Mach number of 0.65. The non-AMR computational grid consisted of 52 grid zones with a total of 221 million points. The results of our findings are discussed in the next section.

C. Automatic Vortex Core Radius Extraction

In the present study, several methods are evaluated for choosing the set of grid points to extract the vortex core radius. The outcome of each method is a set of selected grid points on the view plane. Then, at each selected grid point, the pertinent cross-flow velocity component is computed for two orthogonal axes with a common origin at the selected grid point. The vortex core radius is then plotted as a scalar field using color map contours on the view plane.

The first approach for generating this color map is to choose all grid points in the view plane. Although this approach is straightforward, the resulting core radius color map is difficult to understand. Figure 3a shows a typical result using this approach for the baseline experimental case using the non-AMR grid. This approach performs a vortex core radius computation at every view-plane grid point regardless of whether or not a vortex core is present. Thus, many of the color responses are incomprehensible.

Another approach is to extract the vortex core radius only at grid points where the vorticity magnitude is above a threshold value. Figure 3b shows the outcome of applying a threshold value to the same dataset as used in Fig. 3a. Though the results are improved, the disadvantage of the second approach is that the user needs to specify a threshold. An additional difficulty is that certain grid points have a high vorticity because of their proximity to the rotor blade wake as shown in Fig. 3b.

A preferable approach is to eliminate the specification of a threshold altogether. Any scalar quantity, such as vorticity magnitude or the Q criterion,[12] can be used in the user-specified-threshold approach described above. In the present study we adopt a scaled Q-criterion quantity, which is non-dimensional.[12] The Q criterion and the scaled Q criterion are defined by the following equations, respectively, where Ω is the rotation rate tensor and S is the strain rate tensor:

$$Q = \frac{1}{2}(\|\Omega\|^2 + \|S\|^2)$$

$$Q_s = \frac{1}{2}\left(\frac{\|\Omega\|^2}{\|S\|^2} + 1\right)$$

The advantage of using the scaled Q criterion is that a threshold value of 1 gives a good approximation of the vortex core boundary. By calculating the vortex core radii at grid points where the scaled Q criterion is greater than or equal to 1, a vortex core color map is automatically created that gives a clear delineation of the vortex strength across the PIV plane. Figure 4 shows a color map of the vortex core radius based on the scaled Q criterion. In comparison to Fig. 3b, Fig. 4 gives a better depiction of each vortex core. Compared to Fig. 3, the number of grid points where the vortex core radius is calculated is smaller. Figure 5a shows an overlay of Fig. 4 with the cross-flow velocity field. As shown, some of the grid locations where the vortex core is extracted are not near a vortex core

center as indicated from the cross-flow velocity field. This implies that using the scaled Q criterion alone is not sufficient for selecting the correct set of vortex cores.

Thus, we propose a modified criterion for choosing the set of grid points to extract the vortex core radius. The proposed criterion is to calculate the variation of the neighboring velocity vectors. The new approach first determines the grid points where the scaled Q criterion is greater than or equal to 1. Then, a smaller subset of these grid points is selected by determining those grid points that have high cross-flow velocity variation, for example, where the angle between two neighboring cross-flow velocity vectors is greater than 15°. The outcome of applying this approach is shown in Fig. 5b. As shown, the set of grid points where the vortex core radius is extracted is smaller than in Figs. 3b and 4.

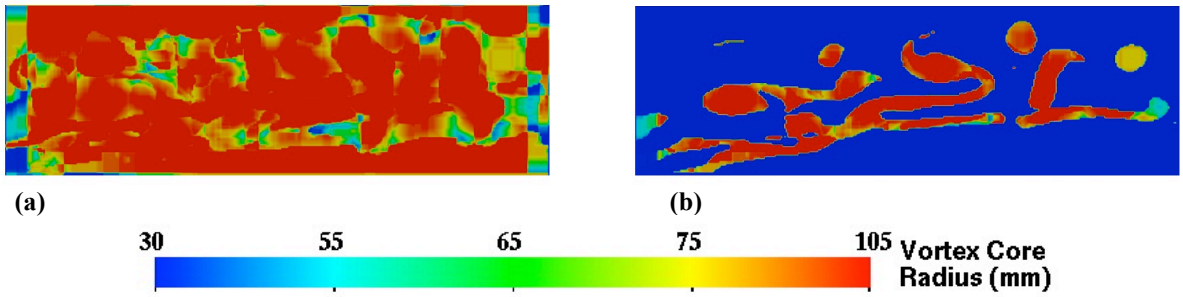

Figure 3. (a) A color map of the vortex core radius on the PIV plane. The core radii are calculated for all grid points on the PIV plane. (b) The core radii are calculated for all grid points on the PIV plane where the vorticity magnitude is greater than 64 s^{-1}.

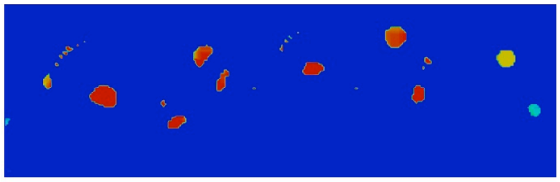

Figure 4. The vortex core radii at the grid points where the scaled Q criterion is greater than or equal to 1.

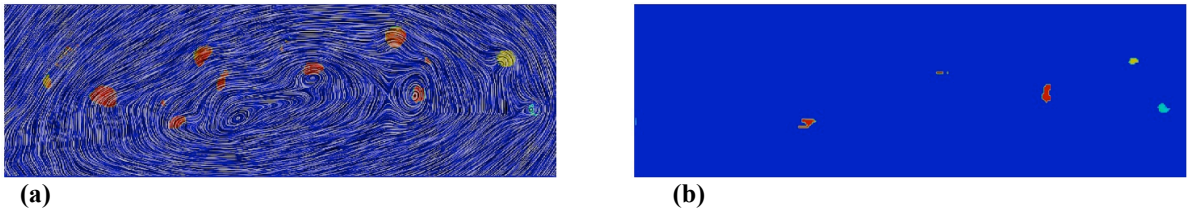

Figure 5. (a) Fig. 4 overlaid with the cross-flow velocity field shows that not all vortex core radii are extracted at actual vortex core centers. (b) The vortex core radii at the grid points where the scaled Q criterion is greater than or equal to 1 and the cross-flow velocity variation is large.

III. Results

Our approach described in the previous section is now applied with an emphasis on examining flow field physics for two case studies involving an isolated UH-60A rotor system.[7] Both case studies are based on Run 73 from Ref. 1, which is one of the test conditions under which PIV data were acquired. Run 73 is a low-speed flow with significant Blade Vortex Interaction (BVI). Some of the important parameters for this case are: the advance ratio $\mu = \frac{M_\infty}{M_{tip}} = 0.15$, the freestream Mach number $M_\infty = 0.0975$, and the tip Mach number $M_{tip} = 0.65$. The main objective of these case studies is to validate computational results and to understand flow structure interactions in the rotor wake.[7]

A. Case Study 1

The first case involves an isolated rotor in free air, with flow conditions taken from Ref. 1, Run 73. Results from two gridding systems are shown: a non-AMR grid with a fixed L1 grid resolution of 5% C_{tip} and an AMR grid system with L1 grids that range from 10% C_{tip} to 2.5% C_{tip}, where the parameter C_{tip} is the rotor blade tip chord length. See Table 1 for a tabulation of information for these two grids.

Gridding System	Number of Grids	Total Grid Points	L1 Spacing
Non-adaptive	124	124 million	0.05 C_{tip}
Adaptive	12,239	725 million	0.10, 0.05, 0.025 C_{tip}

Table 1. Grid statistics for the two cases used in the spatial sensitivity case study.

Figure 6a shows a top view of the computed vortex wake represented by Q-criterion iso-surfaces, which provides a convenient way to visualize vortices.[13] The relative position of the PIV plane is also shown. The angle between the PIV plane and the primary blade 1 is called the delayed azimuth or $\Delta\psi_1$. Figure 6b depicts vorticity magnitude contours in the PIV plane for the flow shown in Fig. 6a. Tip vortices from three blades, Blade 1, Blade 3 and Blade 4, are identified in Fig. 6b. Note that Blade 4 is 90° ahead of Blade 1, and Blade 3 is 180° ahead of Blade 1.

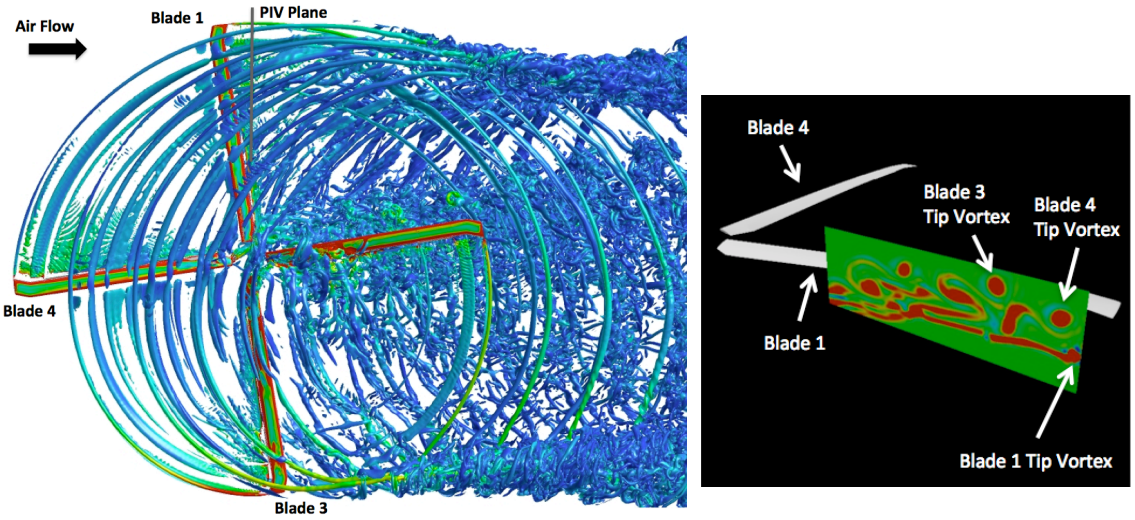

(a) **(b)**

Figure 6. (a) A top view of the vortex wake represented by Q-criterion iso-surfaces. $M_{tip} = 0.65$, $\mu = 0.15$. (b) Vorticity magnitude contours on the PIV plane.

Figure 7a shows a plot of the PIV plane colored by the vorticity at $\Delta\psi_1 = 5°$ (that is, Blade 1 is at 95° azimuth). Figure 7b shows a plot of the PIV plane colored by the vortex core radius, using the new scheme presented above and a threshold value of 64 s^{-1}. As seen, the vortex core radii are computed only at points where the vorticity is above the threshold. It can also be seen that the vortex core radius at Blade 1 (B1) is approximately 55 mm, and the core radius at Blades 3 and 4 (B3 and B4) range between 75 mm to 120 mm. To comprehend a vortex radius color map such as that shown in Fig. 7b, one needs to be knowledgeable of the rotorcraft wake structure that is being analyzed. Using a banded color bar such as the one shown in Fig. 7b, it is much easier to quantify the vortex core radius from the three blade tips.

Figure 8a shows a plot of the PIV plane colored by the scaled Q criterion. Compared to Fig. 7a, Fig. 8a provides a more concise representation of the vortical flow field. Furthermore, it is not necessary to guess the threshold when using the scaled Q criterion. Figure 8b delineates the vortex core radii computed at grid points where the scaled Q criterion is greater than or equal to 1. In comparison with Fig. 7b, Fig. 8b reveals a narrower range of values for the B1, B3, and B4 vortex core radii. However, there are vortex core radii still being extracted for points near the inboard of the rotor blades even though there are no vortices present.

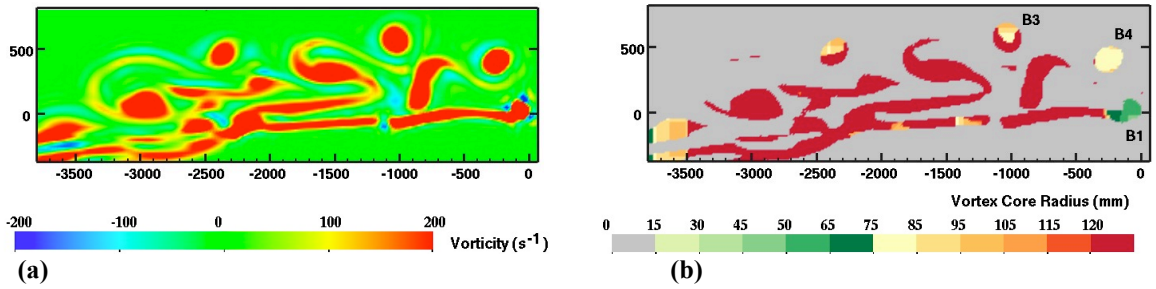

Figure 7. (a) The PIV plane colored by vorticity at a delayed azimuth of 5°, with the flow solution for a UH-60A rotor in forward flight (Run 73, $M_{tip} = 0.65$, $\mu = 0.15$). (b) The PIV plane colored by the vortex core radius where the vorticity magnitude is greater than 64 s^{-1}.

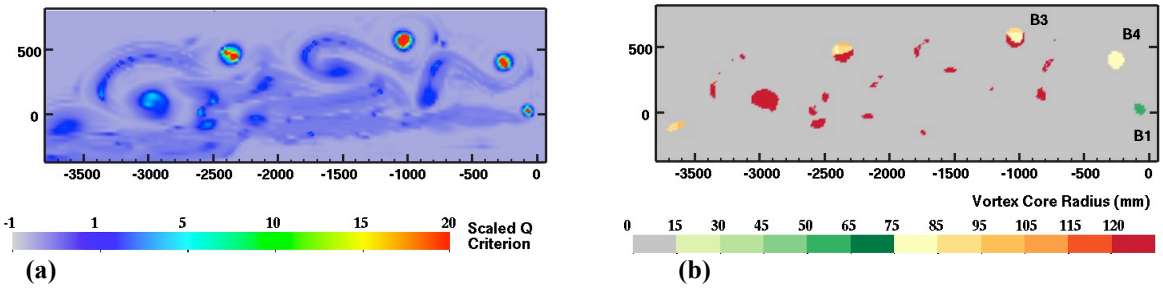

Figure 8. (a) The PIV plane colored by the scaled Q criterion at a delayed azimuth of 5°, with the same data set as used for Fig. 7. (b) The PIV plane colored by the vortex core radius where the scaled Q criterion is greater than or equal to 1.

Figure 9a shows the vortex core radius at points where the scaled Q criterion is greater than or equal to 1 and where there is a large cross-flow velocity variation. Figure 9b depicts a close-up view of Fig. 9a along with the velocity vectors to more clearly delineate the vortex centers. With this additional criterion, the vortex core radius contour map shown in Fig. 9a reveals a concise representation of vortex core attributes (centers and strengths).

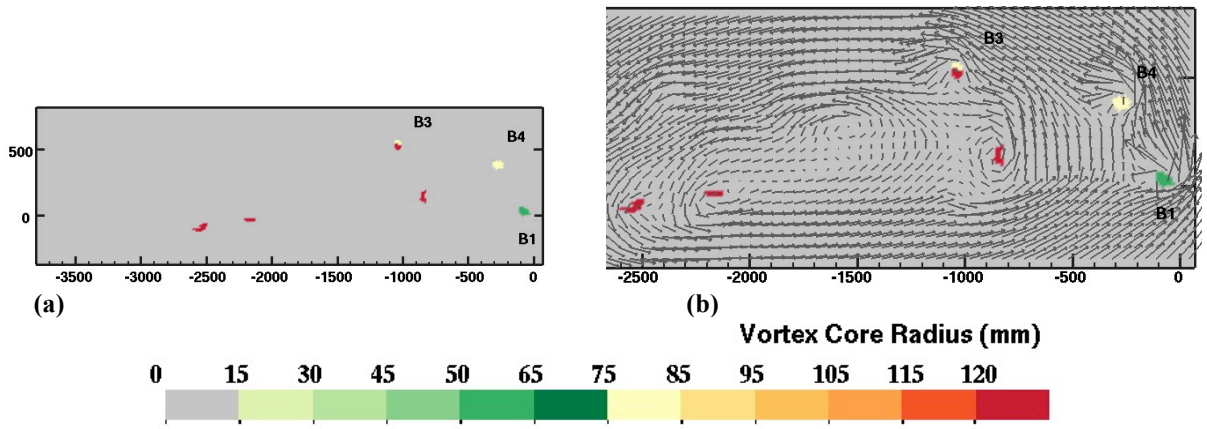

Figure 9. (a) The PIV plane colored by vortex core radius where the scaled Q criterion is greater than or equal to 1 and the cross-flow velocity variation is large. (b) A close-up view with cross-flow velocity vectors (scaled in length).

Next, the flow field generated using an AMR gridding system, consisting of 12,239 grid zones and a total of 725 million grid points (see Table 1), is examined. As shown in Fig. 10, the simulation data using the AMR approach reveals many fine flow field details that were not captured in the previous (non AMR) data set. With this level of grid refinement, various vortex core properties, including the vortex core radius growth with wake age, are in quantitative agreement with experiment.[7] Figures 11a and 11b show comparisons of the computed and measured vorticity contours for the non-adaptive and the AMR simulations, respectively. Figure 11a was generated by first applying an edge detection filter to the image from Fig. 7a to extract computed vorticity contour outlines (shown in magenta). Next, the magenta outlines were overlaid over the experimental vorticity contour outlines (shown in black). This method of comparing the measured and computed vorticity contour outlines provides a better visual comparison of the vorticity contours than using the conventional side-by-side comparison, in which subtle differences are difficult to detect. Figure 11b was generated in a similar fashion using the vorticity contours from the AMR solution. As shown in Figs. 11a and 11b, the high vorticity locations do not differ significantly between the computed and measured results. A closer examination shows that the B1, B3, and B4 vortex core properties match closely between the measured results in core radius and position. The vortex wake structure from the advancing blade is also in good agreement.

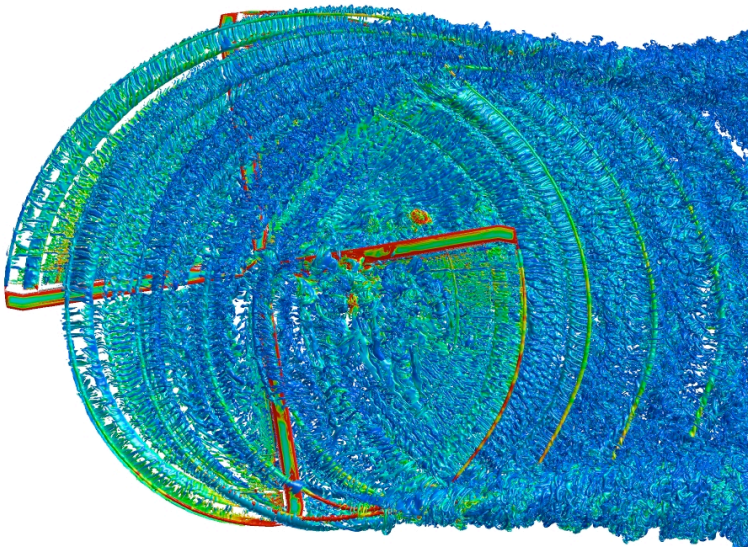

Figure 10. The vortex wake represented by Q-criterion iso-surfaces using an AMR gridding system. M_{tip} = 0.65, M_∞ = 0.0975, μ = 0.15.

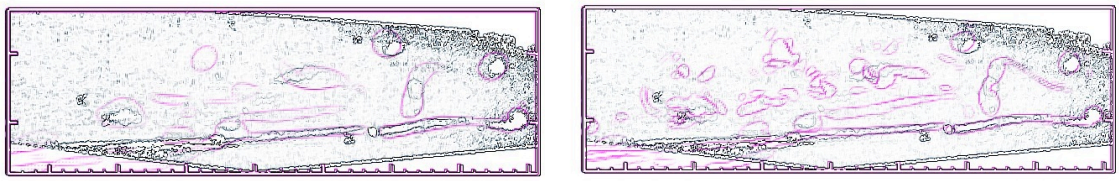

(a) **(b)**

Figure 11. (a) Computed and measured vorticity contours for the non-AMR grid. (b) Computed and measured vorticity contours for the AMR grid.

Figure 12a shows vorticity contours plotted in the PIV plane for the AMR grid. Note the increased resolution available with the refined grid relative to the same view using the standard grid (Fig. 7a). Figure 12b shows a plot of the PIV plane colored by the vortex core radius. Vortex core radii are computed at points where the vorticity is above 64 s^{-1}. As seen in the figure, the vortex core radius for Blade 1 (B1) is approximately 50 mm. For Blades 3 and 4 (B3 and B4) the vortex core radii are approximately 55 mm.

Figure 13a shows a plot of the PIV plane colored by the scaled Q criterion. Figure 13b shows the vortex core radii computed at grid points where the scaled Q criterion is greater than or equal to 1, which reveals a smaller range of vortex core values for B1, B3 and B4 than in Fig. 8b. Due to grid refinement, additional small flow features are revealed as shown in Fig. 13b, especially near the inboard section of the rotor blade. By eliminating grid points that do not have high velocity variation, Fig. 14a shows a smaller subset of the Fig. 13b flow features and gives a more concise representation of the vortex core. Figure 14b depicts an enlarged view showing cross-flow velocity vectors in the tip flow region overlaid onto Fig. 14a to give a better depiction of the vortex core centers.

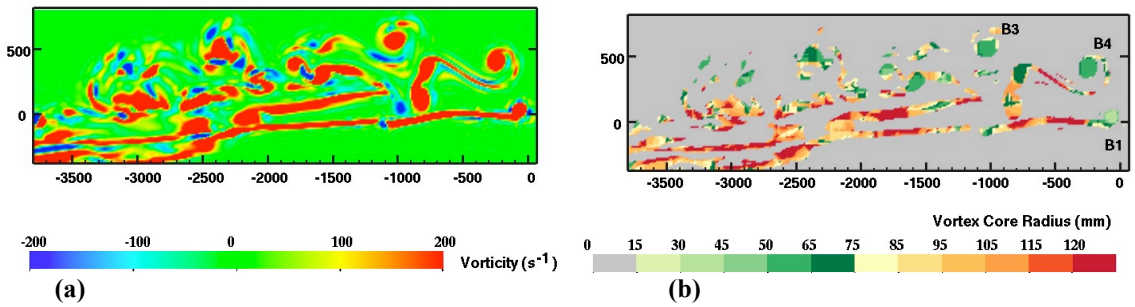

Figure 12. (a) Vorticity contours plotted in the PIV plane at a delayed azimuth of 5°, for a UH-60A rotor in forward flight (Run 73, M_{tip} = 0.65, μ = 0.15). (b) Vortex core radius plotted in the PIV plane where the vorticity magnitude is greater than 64 s^{-1}.

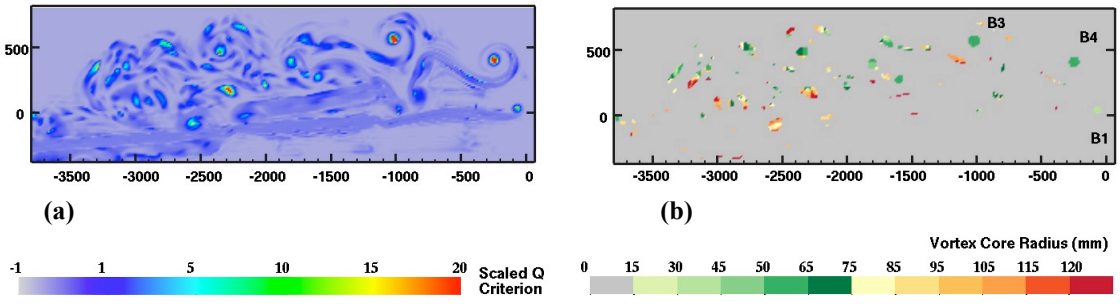

Figure 13. (a) The PIV plane colored by the scaled Q criterion at a delayed azimuth of 5° with the same data set used for Fig. 12. (b) The PIV plane colored by the vortex core radius where the scaled Q criterion is greater than or equal to 1.

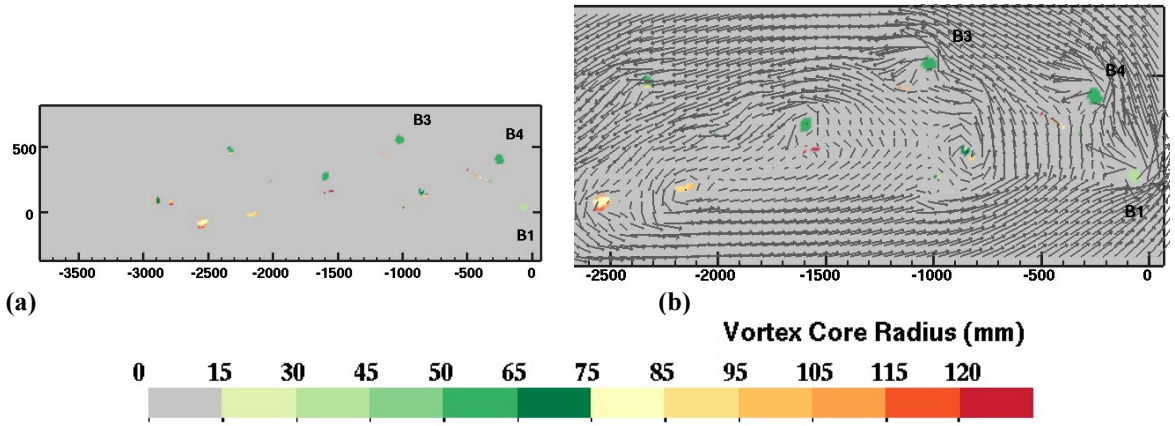

Figure 14. (a) The PIV plane colored by the vortex core radius where the scaled Q criterion is greater than or equal to 1 and the cross-flow velocity variation is large. (b) An enlarged view showing cross-flow velocity vectors (scaled in length) in the tip flow region of Fig. 14a.

B. Case Study 2

This case is similar to case 1 except the fuselage (Large Rotor Test Assembly) is included in the simulation.[14] Simulations were performed for two flow conditions: (a) free air and (b) with wind tunnel walls modeled. The purpose of this case study is to determine the effect of wind tunnel walls as well as the rotor-fuselage on the flow solution. The grid system for the free air simulation consists of 136 grid zones and approximately 403 million grid points. The grid system for the wind-tunnel-wall simulation consists of 36 grid zones and approximately 299 million grid points. Both grid systems have 0.05 C_{tip} spacing in the finest L1 grids (see Table 2).

Simulation Type	Number of Grids	Total Grid Points	L1 Spacing
Free Air	136	403 million	0.05 C_{tip}
Wind Tunnel Walls	36	299 million	0.05 C_{tip}

Table 2. Grid statistics used for the flow simulations with and without wind tunnel wall modeling.

Figures 15a and 15b compare the vortex wake from the free air simulation versus the simulation with wind tunnel walls modeled. In these two figures, Q-criterion iso-surfaces are compared. From the case study analysis, it was found that the inclusion of the wind tunnel walls in the simulation did not make a significant difference in the general flow simulation results. This is further validated in Figs. 16 and 17. Figure 16 shows a comparison of the computed and measured vorticity contours for the free air simulation (Fig. 16a) and the simulation with wind tunnel walls modeled (Fig. 16b). Figure 17 shows vorticity contours in the PIV plane for the same two comparisons. As shown in Fig. 17, the vorticity contours for the free air simulation and the simulation with wind tunnel walls are relatively similar. The blade tip vortices (B1, B3 and B4) are also in good agreement. Figures 16a and 16b were generated by extracting vorticity contour outlines from Figs. 17a and 17b using an edge detection filter, respectively. The computed vorticity contour outlines in Fig. 16 are shown in magenta and the measured vorticity contour outlines are shown in black. An analysis of the results from Figs. 16 and 17 indicates that there is not a significant difference in vortex position and strength, especially near the blade tip, for these two simulations.

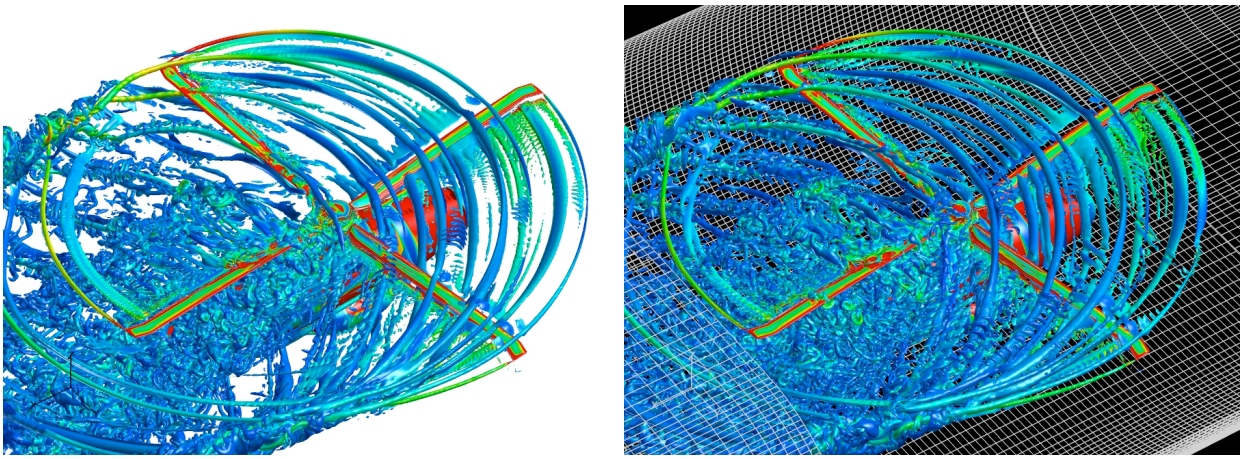

(a) (b)

Figure 15. (a) Vortex wake represented by Q-criterion iso-surfaces for the free air simulation. (b) Vortex wake represented by Q-criterion density iso-surfaces for the simulation with wind tunnel walls (white background grid is at the lower wind-tunnel wall surface). (Run 73, $M_{tip} = 0.65$, $\mu = 0.15$).

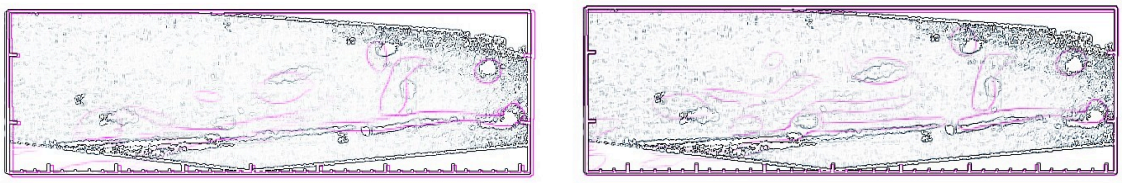

(a) (b)

Figure 16. (a) Computed and measured vorticity contours for the free air simulation. (b) Computed and measured vorticity contours for the simulation with wind tunnel walls. The computed vorticity contours are in magenta. The experiment results are in black.

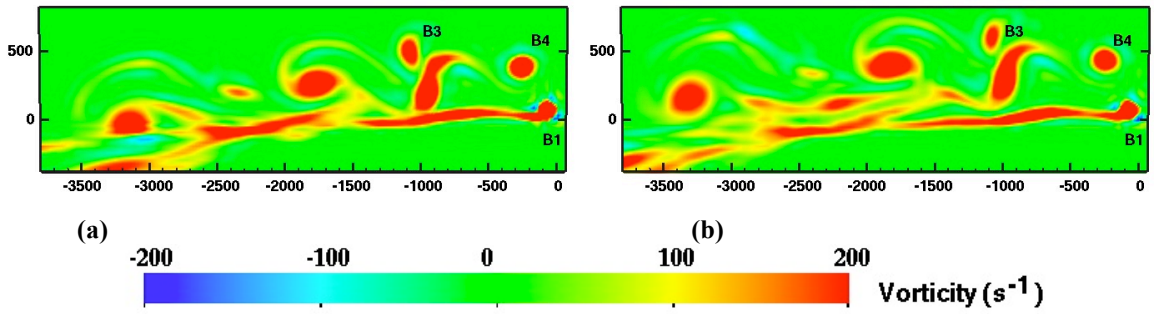

Figure 17. (a) Vorticity contours for the free air simulation. (b) Vorticity contours for the simulation with wind tunnel walls.

Figure 18 shows scaled Q-criterion contours in the PIV plane for the free-air and the wind-tunnel-wall simulations. Similar to the results shown in Fig. 17, the scaled Q-criterion contour comparison shows only a few minor variations between the two different cases, and these differences are primarily near the inboard section of the rotor blade.

Figure 19 shows color contour maps of vortex core radii on the PIV plane (enlarged view) where the scaled Q criterion is greater than or equal to 1 and the cross-flow velocity variation is large. Figure 19a shows a result for the free-air case, and Fig. 19b shows the result for the wind-tunnel-wall case. To validate the locations of each vortex core, the velocity vectors from experiment are also shown. As expected, there is only a slight difference in the vortex core radii contour maps between the free-air and the wind-tunnel-wall simulations. Furthermore, the B3 blade tip vortex shown in Fig. 17 does not appear in Fig. 19. A possible explanation is that there is a large vortex structure below the B3 vortex core hence the cross-flow velocity variation is not large enough to meet the criterion for choosing the set of grid points to extract the vortex core radius.

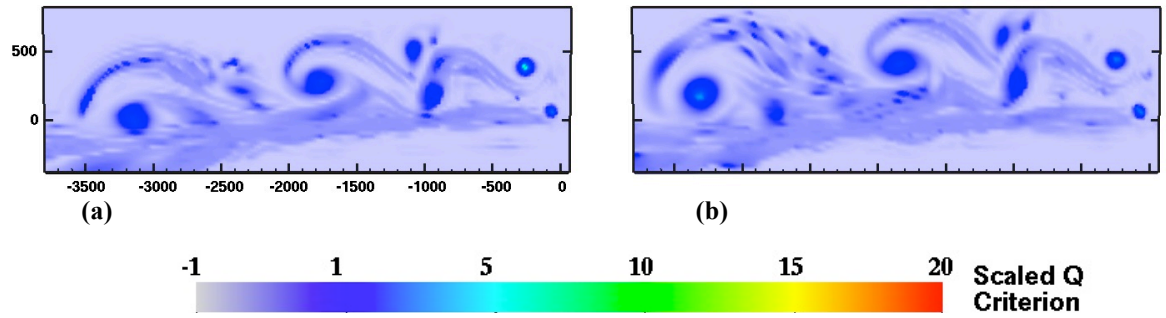

Figure 18. (a) Scaled Q-criterion contours for the free air simulation. (b) Scaled Q-criterion contours for the simulation with wind tunnel walls.

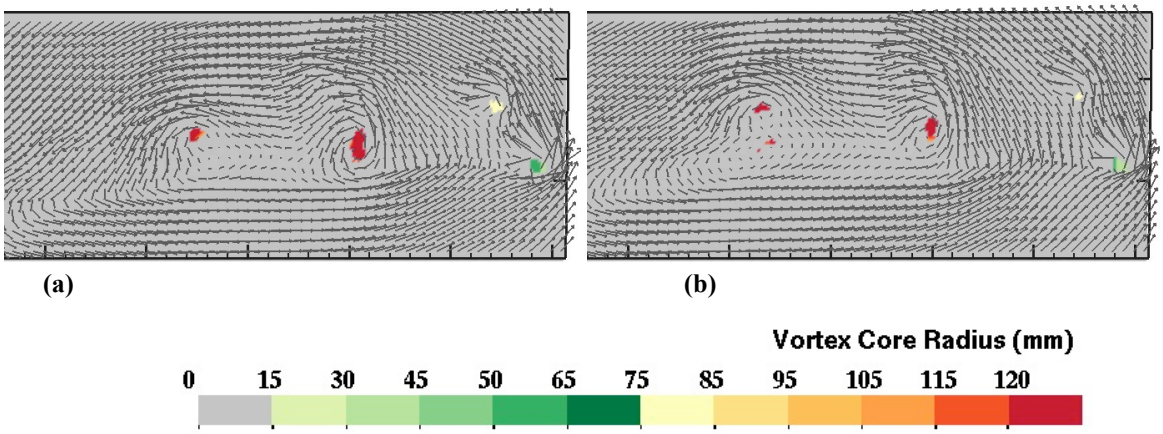

Figure 19. Vortex core radii computed at points where the scaled Q criterion is greater than or equal to 1 and the cross-flow velocity variation is large. (a) Free air simulation and (b) With wind tunnel walls.

C. Implementation Details

The presented approach was implemented in an in-house software program called VCE (Vortex Core Extraction) that is currently under development. VCE is implemented using C and FORTRAN programming languages. For a given time step, a pre-processing of the associated grid file is performed to determine which grids intersect the PIV plane. A grid ID file that contains the grid number of each intersecting grid is then created. The time required to perform this pre-processing step depends on the number of grids. For an AMR gridding system with tens of thousands of grids, it will take a few minutes to perform this task. For a non-AMR grid, the pre-processing time is much faster. During execution VCE reads this ID file along with the actual grid and solution files to construct the view plane. Next, the scaled Q-criterion scalar field is computed. Then, VCE calculates the vortex core radius by performing the cross-flow velocity profiling at those grids that meet the selection criterion. The entire procedure is fully automatic without requiring any user input. The time that it takes to compute and extract the vortex core radius is less than one minute of wall clock time.

VI. Summary

An automated approach for extracting and quantifying rotor tip vortex strength has been presented. The approach was demonstrated on CFD simulations from two case studies for a UH-60A rotor in forward flight. Two criteria were evaluated for selecting grid point locations to perform the automatic vortex core profiling and vortex core radius calculations. Each selection criteria is fully automated and does not require user intervention. A new scheme utilizing the vortex core radius as a scalar field was presented, which allowed the display of the vortex core radius information on the experimental PIV plane. Color map contours based on vortex core radius provide a concise representation of the vortex core strength when compared to traditional scalar quantities such as vorticity magnitude.

Acknowledgments

This work was sponsored by the Rotorary Wing Project within the NASA Fundamental Aeronautics Program.

References

[1]Yamauchi, G.K., Wadcock, A.J., Johnson, W., and Ramasamy, M., "Wind Tunnel Measurements of Full-Scale UH-60A Rotor Tip Vortices," AHS 68th Annual Forum, May 2012.

[2]Bhagwat, M.J. and Leishman, J.G., "Correlation of Helicopter Rotor Tip Vortex Measurements," AIAA Journal, Vol. 38, No. 2, 2000, pp. 301-308.

[3]Leishman, J.G. and Bhagwat, M., "Challenges in Understanding the Vortex Dynamics of Helicopter Rotor Wake," *AIAA Journal,* Vol. 36, No., 7, 1998, pp. 1130-1140.

[4]McAlister, K. and Heineck, J., "Measurements of the Early Development of Trailing Vorticity from a Rotor," NASA/TP-2002-211848, AFDD/TR-02-A001, May 2002.

[5]Mula, S.M., Stephenson, J., Tinney, C.E., and Sirohi, J., "Vortex Jitter in Hover," AHS Southwest Region Technical Specialist's Meeting, February 2011.

[6]Ramasamy, M. and Paetzel, R., "Aperiodicity Correlation for Rotor Tip Measurements," AHS 67th Annual Forum, May 2011.

[7]Ahmad, J.U., Yamauchi, G.K., and Kao, D.L., "Comparison of Computed and Measured Vortex Evolution for a UH-60A Rotor in Forward Flight," 31st AIAA Applied Aerodynamics Conference, AIAA Paper 2013-3160, June 2013.

[8]Kao, D.L. and Chaderjian, N.M., "Automatic Tip Vortex Core Profiling for Numerical Flow Simulations of Rotorcraft in Hover," 40th AIAA Fluid Dynamics Conference, AIAA Paper 2010-4752, June 2010.

[9]Kao, D.L, "Automatic Vortex Core Analysis for Multi-Zone Numerical Flow Simulations," 20th AIAA Computational Fluid Dynamics Conference, AIAA Paper 2011-3679, June 2011.

[10]Meakin, R., "Moving Body Overset Grid Methods for Complete Aircraft Tiltrotor Simulations," AIAA Paper 1993-3350, 1993.

[11]Nichols, R., Tramel, R., and Buning, P., "Solver and Turbulence Model Upgrades to OVERFLOW 2 for Unsteady and High-Speed Flow Applications," AIAA-2006-2824, June 2006.

[12]Kamkar, S.J., Wissink, A.M., Sankaran, V., and Jameson, A., "Feature-driven Cartesian Adaptive Mesh Refinement for Vortex-Dominated Flows," Journal of Computational Physics, Vol. 230, No. 16, 2011, pp. 6271-6298.

[13]Ahmad, J. and Chaderjian, N., "High-Order Accurate CFD/CSD Simulation of the UH-60 Rotor in Forward Flight," AIAA Paper 2011-3185, 29th Applied Aerodynamics Conference, June 2011.

[14]Ahmad, J. U., personal communications.